NANO LETTERS

Letter

pubs.acs.org/NanoLett

Detection of Charges and Molecules with Self-Assembled Nano-Oscillators

Xiaonan Shan,[†] Yimin Fang,[‡] Shaopeng Wang,[†] Yan Guan,[†] Hong-Yuan Chen,[‡] and Nongjian Tao*[,†,‡]

[†]Center for Bioelectronics and Biosensors, Biodesign Institute, Arizona State University, Tempe, Arizona 85287, United States

[‡]State Key Laboratory of Analytical Chemistry for Life Science, School of Chemistry and Chemical Engineering, Nanjing University, Nanjing 210093, China

Supporting Information

ABSTRACT: Detection of a single or small amount of charges and molecules in biologically relevant aqueous solutions is a long-standing goal in analytical science and detection technology. Here we report on self-assembled nano-oscillators for charge and molecular binding detections in aqueous solutions. Each nano-oscillator consists of a nanoparticle linked to a solid surface via a molecular tether. By applying an oscillating electric field normal to the surface, the nanoparticles oscillate, which is detected individually with ∼0.1 nm accuracy by a plasmonic imaging technique. From the oscillation amplitude and phase, the charge of the nanoparticles is determined with a detection limit of ∼0.18 electron charges along with the charge polarity. We further demonstrate the detection of molecular binding with the self-assembled nano-oscillators.

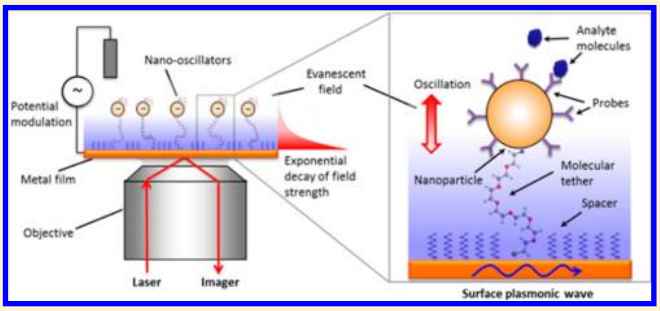

KEYWORDS: *Nano-oscillators, surface plasmon resonance, single charge detection, small molecule detection, plasmonic imaging technique*

Charge is one of most fundamental physical properties of molecules.[1−5] The ability of detecting single or small amount of charges and molecules represents the ultimate limit in analytical science. This has a profound impact on detection technologies, chemical analysis, and sensors.[6−13] Millikan detected single electron charge based on measuring forces on oil droplets 100 years ago.[14] Roukes et al.[15,16] achieved single charge sensitivity using a novel nanoelectromechanical system (NEMS). The oil drop experiment was performed in air, and the NEMS experiment was carried out in vacuum at low temperatures. Detection of the charge of a nanoscaled object with high sensitivity in aqueous solution is significantly more challenging. Recently, Krishnan et al.[17] developed a geometry-induced electrostatic trapping method to trap and detect the charges of the nanoscale objects.[18] The method is based on statistical analysis of the Brownian motion of the objects and requires ultralow ionic strengths, which is not suitable for detection of biologically relevant molecules. We have demonstrated the ability to measure the surface charge density of a surface by using the electrostatic interaction of floating microbeads[19] or electrochemical impedance microscope.[20] Both methods measure the charge on a large surface and cannot be applied to measure a single or a few charges. Here we report self-assembled nano-oscillators for charge and molecular binding detections in aqueous solutions. Each nano-oscillator consists of a nanoparticle linked to a solid chip surface via a molecular tether. By applying an oscillating electric field normal to the surface, the nanoparticles oscillate, which is detected individually with ∼0.1 nm accuracy by a plasmonic technique. From the oscillation amplitude and phase, the charge of the nanoparticles is determined with a detection limit of ∼0.18 electron charges along with the charge polarity. We further report the detection of molecular binding with the self-assembled nano-oscillators. This self-assembled nano-oscillator allows us to detect small molecules via their charges, which is significant because of the difficulty of detecting small molecules with the traditional technologies.

Each of the nano-oscillators consists of a gold nanoparticle (AuNP) attached to a gold substrate via a molecular tether, such as polyethylene glycol (PEG) terminated with proper linker groups (Figure 1a). An alternating (AC) electric field is created perpendicular to the gold substrate by applying an AC voltage between the substrate and a reference electrode inserted in the solution. The nanoparticle, when charged, oscillates with the electric field.[21−23] The molecular tether (PEG) was chosen to be soft such that it can be stretched from a relaxed configuration to its fully stretched linear configuration under a relative small driving force. This ensures large oscillation amplitude and thus accurate charge sensitivity.

The oscillation amplitude of each oscillator is detected individually by a surface plasmon resonance imaging technique[24−27] (Figure 1b). The technique creates a planar

Received: May 14, 2014
Revised: June 12, 2014

   dx.doi.org/10.1021/nl501805e | *Nano Lett.* XXXX, XXX, XXX−XXX

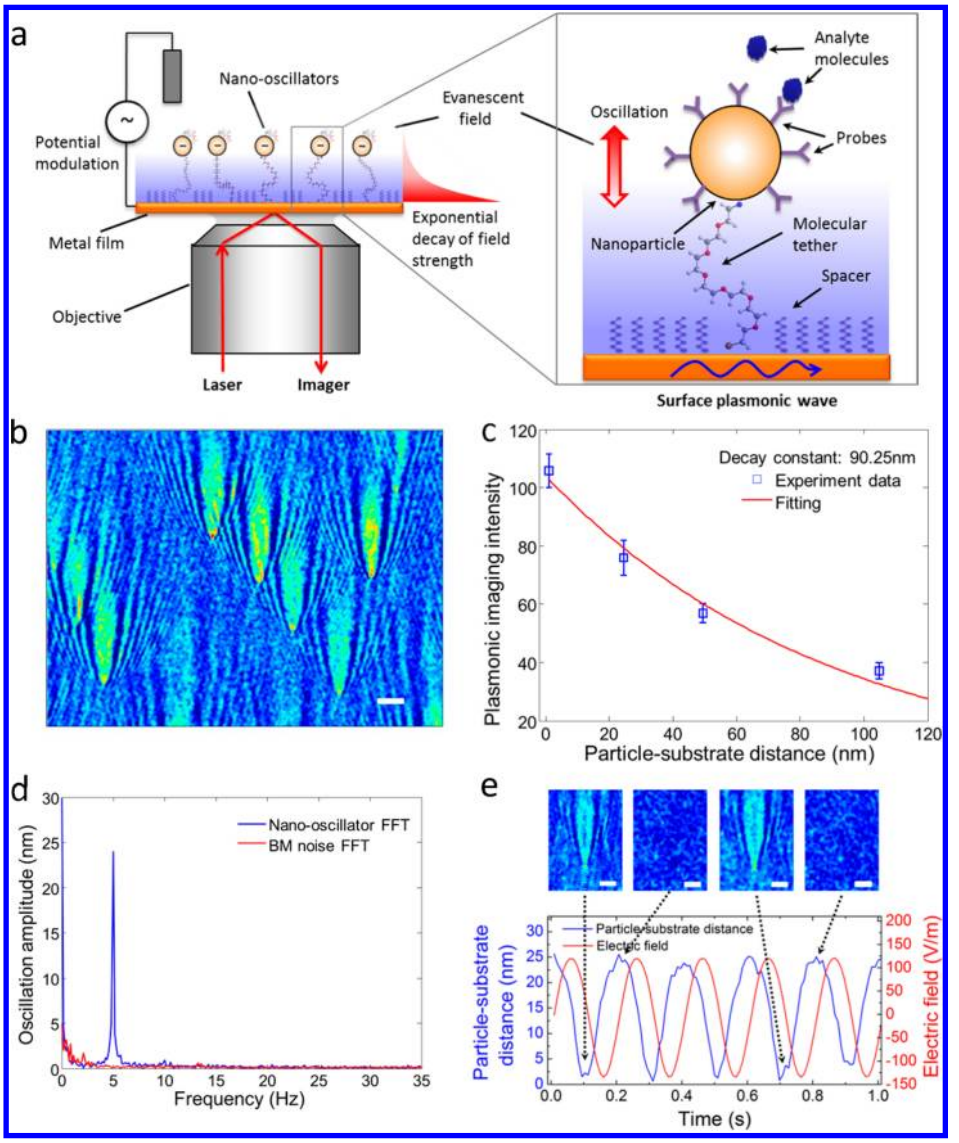

Figure 1. (a) Schematic illustration of nano-oscillators self-assembled on a Au-substrate and plasmonic imaging of their oscillations. Each nano-oscillator consists of a AuNP and a soft molecular tether attached to the substrate. The figure on the right side has shown the zoomed in area in the left side image, and molecular structure of PEG tether molecule has been drawn. Note that for clearance purpose, not all the polyethylene glycol repeating subunits are shown in the figure on the right side. The dark yellow, red, white, and blue dots represent thiol, carbon, hydrogen, and biotin atoms or molecules, respectively. (b) Plasmonic image of individual nano-oscillators (30 nm diameter AuNP, PEG molecular tether with molecular mass of 3400 g/mol and linear length of 33 nm. Scale bar, 5 μm. (c) Plasmonic image intensity of a nano-oscillator as a function of AuNP−substrate distance. (d) Fourier spectrum of the oscillation amplitude of a nano-oscillator (blue curve) showing a peak at 5 Hz, the frequency of the applied electric field. The equivalent noise due to the Brownian motion (red curve, Fourier spectrum from a nano-oscillator without any potential modulation) at 5 Hz is 0.08 nm. (e) Oscillation of a nano-oscillator (blue) and corresponding driving electric field (red) in time domain. Snapshots of several plasmonic images during the oscillation are shown (top). Scale bar: 5 μm. The experimental condition used in (d,e) is 1 mM phosphate buffer with applied electric field amplitude of ∼137 V/m and frequency of 5 Hz.

surface plasmon wave on the gold substrate, and the presence of a AuNP scatters the plasmonic wave, leading to a parabolic shape pattern in the image.[27,28] The evanescent field associated with the surface plasmons decays exponentially from the gold substrate into the solution,[29,30] resulting in an extremely sensitive dependence of the plasmonic image intensity on the nanoparticle oscillation amplitude (Figure 1c). The imaging technique allows us to detect the amplitude of each nano-oscillator with an accuracy of ∼0.1 nm (Figure 1d) (see Supporting Information). This high accuracy leads to precise monitoring of the charge of each nanoparticle as well as random fluctuations in the charge over time. Note that accurate distance between a metal nanoparticle and a gold film has been determined by analyzing optical absorption spectrum of localized SPR in the nanoparticle.[31,32] Unlike the localized SPR, the present approach works for both metallic and dielectric nanoparticles and is fast to allow tracking of rapid oscillation.

When molecules bind to the nano-oscillators, the effective charge changes, which can be monitored in real time, such that each nano-oscillator acts as a nanosensor for detection of molecular binding processes. A high-density array of such nanosensors (e.g., 100 000 per mm^2) can be self-assembled onto the gold surface in aqueous solution, which can be driven into oscillation and detected in parallel with the plasmonic

dx.doi.org/10.1021/nl501805e | Nano Lett. XXXX, XXX, XXX−XXX

imaging method, thus promising a potential for high throughput study of molecular interactions.[33−37]

The AuNPs with diameter 30 nm were coated with streptavidin and the substrate was prepared by coating a microscope cover slide with 47 nm Au film. A molecular tether (PEG with molecular weight of 3400) was used to link each AuNP to the substrate. Each molecular tether was terminated with a biotin on one end to link the streptavidin coated AuNPs and a thiol on the other end to bind onto the gold substrate (Figure 1a). In order to control the density of the nano-oscillators, the molecular tethers were mixed with thiol-PEG_4-OCH_3 spacers with appropriate ratios before self-assembly onto the gold substrate. In addition to serving as spacers between the individual molecular tethers, the thiol-PEG_4-OCH_3 molecules also block nonspecific adsorption of AuNPs directly onto the gold substrate and reduce charging effect that arises from the dependence of the surface plasmons resonance on the surface charge density.[27] To avoid multiple tether molecules binding to one particle, the ratio of tether molecule and spacer molecule was carefully controlled and optimized (see Supporting Information). Note that because the nano-oscillators are over damped, the tether molecule (single or multiple) did not affect the oscillation of the nanoparticles (see eq 1).

The plasmonic detection was carried out on a modified inverted optical microscope with a high numerical aperture objective (Figure 1a).[26] The individual nano-oscillators can be imaged with high contrast because of the scattering of the planar plasmonic waves on the gold surface by the AuNPs of the nano-oscillators. The scattering generates circular plasmonic waves centered at the individual AuNPs, which interfere with the planar plasmonic wave propagating on the surface and form the distinct parabolic shape images of the AuNPs (Figure 1b). The length of parabolic shape is about a few micrometers (for incident light with wavelength of 680 nm), which reflects the propagation length of the surface plasmon wave. The image intensity of AuNP is sensitive to the distance between the AuNP and gold surface.[21,38] To determine the actual distance, we obtained a calibration curve by measuring the image intensity as a function of the AuNP−substrate distance (Figure 1c). The distance was controlled by coating the gold surface with a layer of CYTOP polymer with different thicknesses (Supporting Information, Figure S1a). CYTOP was chosen because its refractive index is 1.34,[39] close to that of the aqueous solution, which can control the distance between a AuNP and the gold substrate without affecting the distribution of the evanescent field. The result for the 30 nm AuNPs is plotted in Figure 1c, which can be fitted with an exponential function with a decay length of 90.3 nm. The decay constant is consistent with a theoretical estimate based on a simplified model presented in the Figure S1b (Supporting Information). Note that the coupling of the local SPR of AuNP with the metal film leads to more complicated intensity versus distance relationship than the simple exponential decay,[40,41] but this complication occurs at a distance (a few nanometers) smaller than the smallest AuNP−substrate distance (determined by the spacer and relaxed molecular length of PEG) in the present work.

To drive the nano-oscillators into oscillation, a sinusoidal electric field normal to the gold surface was created via the standard electrochemical three electrode setup (only two electrodes are shown in Figure 1a for clarity).[38,42,43] The electric field moved the charged AuNPs up and down, which was observed as a periodic oscillation in the image intensity for each AuNP (Supporting Information Movie S1). Figure 1a shows the oscillating image intensity profile (blue curve) of a AuNP over time, together with the applied field (red curve). Note that the linear length of the molecular tethers used in the experiment is ∼33 nm, so the amplitude of the oscillation can vary from 0 to ∼33 nm.

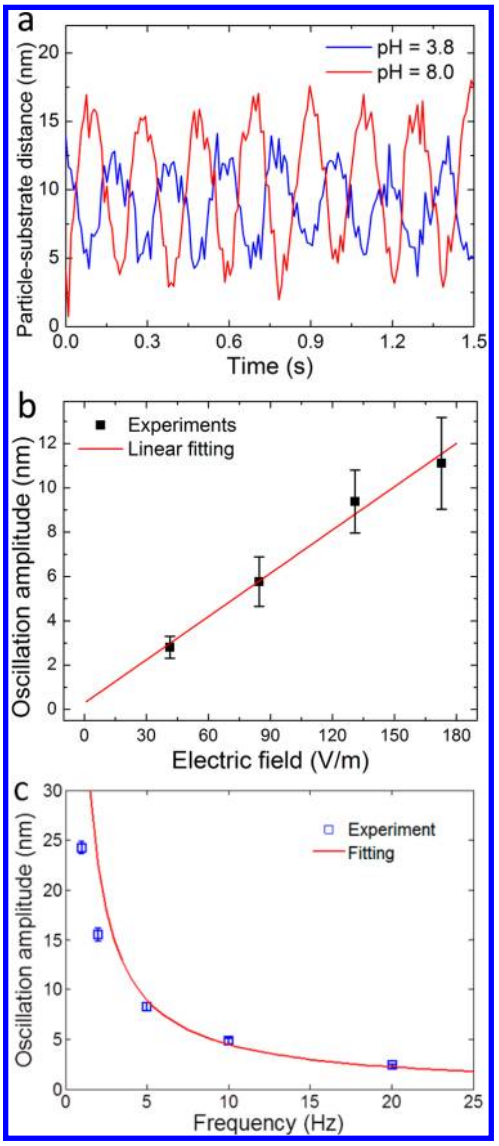

Figure 2. (a) Oscillation of a nano-oscillator in pH = 3.8 (blue) and 8.0 (red) acetate buffer (1 mM). The applied electric field amplitudes are 75 and 100 V/m at pH = 3.8 and 8.0, respectively. (b) Dependence of the oscillation amplitude on the applied electric field amplitude, where the red line is a linear fit to the data. (c) Dependence of the oscillation amplitude on the applied electric field frequency, where the red curve is a fit to the data with eq 1.

A few snapshots of the plasmonic image of the AuNP are shown as insets of Figure 1e. The dynamics of the nano-oscillators can be described by a damped harmonic oscillator model. Because the AuNPs are small and the molecular tethers are soft, both the inertia and spring restoring terms are negligible in the viscous aqueous solution, and the nano-oscillators are thus overdamped (see Supporting Information for more details). This approximation leads to a simplified relation between the displacement amplitude (x_0) of the AuNPs and charge (q), given by

dx.doi.org/10.1021/nl501805e | Nano Lett. XXXX, XXX, XXX−XXX

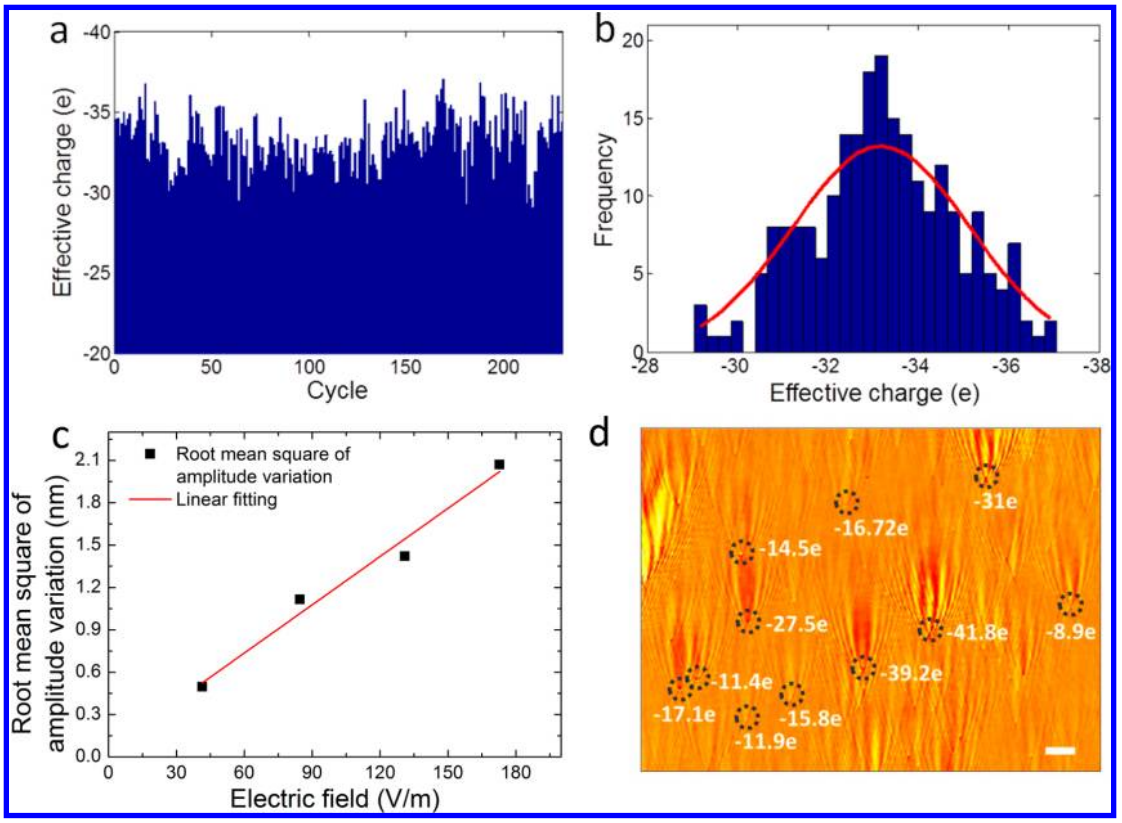

Figure 3. (a) Effective charge of a nano-oscillator (30 nm diameter AuNP) over time (time resolution, 0.2 s per cycle). (b) Histogram of effective charge variations of the nano-oscillator (data from (a)), where the red curve is a Gaussian fit. (c) Relationship between oscillation amplitude fluctuation and applied electric field. (d) Average effective charges for different nano-oscillators. The image was obtained by taking the imaginary part of the Fourier transform for each pixel over 5 s of period. Applied electric field amplitude = 22.75 V/m and frequency = 5 Hz. Buffer: 10 mM phosphate buffer solution. Molecular tether: PEG with molecular mass of 3400 g/mol. Scale bar: 5 μm.

$$x_0 = \frac{E_0}{j12\pi^2\eta a f}q \quad (1)$$

where E_0 and f are the amplitude and frequency of the applied electric field, η is the viscosity of the solution, and a is the radius of AuNP. The relation allows us to determine the charge of the nano-oscillator from the measured oscillation amplitude and phase. Maximum forces exerted on the particles by the electric field estimated from eq 1 is 1 pN (with 300 effective charges under ±0.5 V potential at 5 Hz.). Note that this force is much smaller than the forces that are needed to break long PEG molecules (>300 pN).[44]

In order to validate the working principle, it is essential to examine the predictions of eq 1. The streptavidin-coated AuNPs are negatively charged as confirmed by zeta potential measurement performed under the same buffer condition (Supporting Information). According to eq 1, the oscillation displacement of a negatively charged particle should lead the applied electric field by 90° in phase. The observed phase shift as shown in Figure 1e is ∼94°, which is in good agreement with the model prediction. Detailed analysis of many other AuNPs also shows ∼90° phase shift. Another prediction by eq 1 is that the phase changes by 180° with the charge polarity. To verify this prediction, we measured nano-oscillator response in buffers with different pH values. Because the isoelectric point of streptavidin is between 5 and 6,[45] the AuNPs should be negatively charged for pH > 5−6, and positively charged for pH < 5−6, which has been confirmed by zeta potential measurement as well (see Supporting Information). Figure 2a plots the displacement of a nano-oscillator in buffers with pH = 3.8 and 8.0, respectively, which indeed reveals ∼180° phase shift between the two measurements.

Equation 1 further predicts that the oscillation amplitude is proportional to the amplitude and inversely proportional to the frequency of the applied electric field. To validate these predictions, we measured the nano-oscillators by varying the amplitude and frequency of the applied electric field. The oscillation amplitude increases linearly with the applied electric field as shown in Figure 2b. The relation between the oscillation amplitude and frequency is plotted in Figure 2c, which can be approximately fit with eq 1. At low frequencies (1−2 Hz), it shows some deviations from eq 1, which is because the oscillation amplitude is too large and the molecular tether is stretched to its full limit.

From the measured oscillation amplitude, we can obtain the charge of the AuNPs with eq 1 provided the electric field strength is known. We determined the electric field by measuring the current density of the gold substrate, which is related to the electric field by $J = \sigma E$, where σ is the conductivity of the buffer. From the measured oscillation amplitude and electric field, the effective charge of a single nano-oscillator with 30 nm diameter AuNP was determined in 10 mM PBS buffer over time (Figure 3a). For an oscillation frequency of 5 Hz, the corresponding time resolution was 0.2 s. The average effective charge of the AuNP was found to be −33.2e, where the polarity of the charge was determined from the phase shift.

dx.doi.org/10.1021/nl501805e | Nano Lett. XXXX, XXX, XXX−XXX

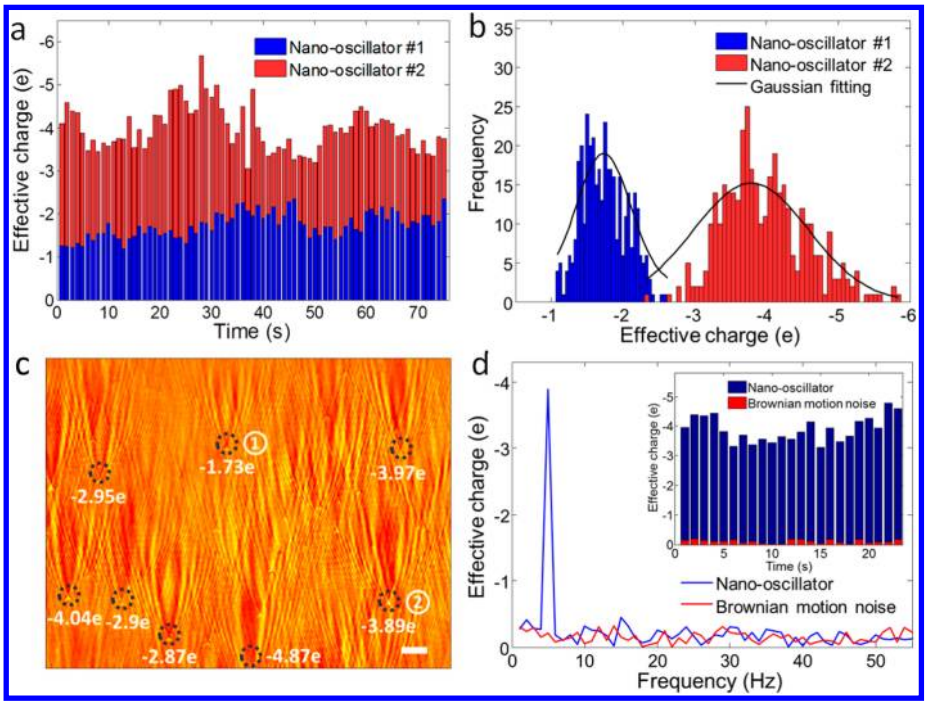

Figure 4. (a) Effective charges of nano-oscillators (#1 and #2 marked in (c)). Solution: acetate buffer with pH = 5.3. (b) Histogram of the charge over time for the two nano-oscillators, where the black curves are Gaussian fittings. (c) Image of effective charges for different nano-oscillators. The image was obtained by taking the imaginary part of the Fourier transform for each pixel over 5 s of period. Scale bar, 5 μm. (d) Fourier spectra of the oscillation (with potential modulation) and Brownian motion (without potential modulation) of a nano-oscillator (data averaged over 1 s). Scale bar: 5 μm. Inset: The effective charge of the nano-oscillator (blue) and equivalent effective charge due to the Brownian motion noise (red) over time (see Supporting Information for details). Applied electric field: amplitude = 137 V/m and frequency = 5 Hz. Molecular tether: PEG with molecular mass of 3400 g/mol. Buffer: 1 mM acetate solution.

The effective charge of the AuNP fluctuated over time as shown in Figure 3a. The charge fluctuations are more clearly shown in a histogram plot in Figure 3b. The distribution can be fit with a Gaussian (red curve) with a standard deviation of ~2.3e. In aqueous solution with a fixed pH, the charge of the AuNP is determined by the dynamic balance between protonation and deprotonation, which is expected to fluctuate with time. For a AuNP with N charges, the random fluctuation in the charge is $\sim\sqrt{N}e$, where N for the AuNP shown in Figure 3a is about 86, determined from the measured effective charge after considering ionic screening in 10 mM PBS[46,47] (see Supporting Information). The estimated charge fluctuation based on the above relation is 9.3e, corresponding to an effective charge fluctuation of ~3e, which agrees well with the experiment result. The observation of charge fluctuations is further supported by the analysis of the fluctuations in the oscillation amplitude as a function of the applied electric field. According to eq 1, the fluctuations in the oscillation amplitude caused by charge fluctuations should be proportional to the applied electric field. Figure 3c plots the root-mean-square of the oscillation amplitude, which indeed increases linearly with the applied electric field.

The plasmonic detection technique allows us to analyze charges of multiple nano-oscillators simultaneously. Figure 3d is the imaginary part of the Fourier transform of the imaging intensity, which is proportional to the charge according to eq 1. It shows the effective charges for 11 nano-oscillators, whose effective charges and locations are labeled with filled circles. The data show that all the AuNPs are negatively charged, but the amount of charges varies over a wide range.

To examine the capability of the self-assembled nano-oscillator method for the detection of a small amount of charges, we tuned the buffer pH to 5.3, close to the isoelectric point of streptavidin so that each AuNP carried only a few charges. We also lowered the buffer (acetate) concentration to 1 mM to decrease the ionic screening effect on the charge. Figure 4a plots the effective charges of two nano-oscillators, 1 (red) and 2 (blue). The effective charge of nano-oscillator 1 is about 1.7e, and the corresponding charge after the correction of the screening effect is 2.3e. In addition to charge screening, another reason for the observed fractional effective charges is time averaging due to the limited bandwidth of the detection (0.2 s for 5 Hz), which could wash out discrete charge fluctuations associated with the fast dynamics of protonation and deprotonation. Note that PEG linkers are uncharged, which should not contribute to the detected charge. The fluctuations in the effective charges of the two nano-oscillators are plotted in Figure 4b with standard deviations of 0.31e and 0.59e, respectively. We have also studied charges of other nano-oscillators. Figure 4c is the imaginary part of the Fourier transform of the imaging intensity, which is proportional to the charge according to eq 1. The image shows that the charges of different AuNPs in pH = 5.3 vary from −1.7e to −4.9e.

The detection limit of the present method is mainly determined by the Brownian motion of the nano-oscillators. Figure 4d plots the noise spectrum of the Brownian motion of a nano-oscillator (red) together with the frequency spectrum of the electric field-driven oscillation of the nano-oscillator (blue curve). The standard deviation of the Brownian motion noise at the oscillation frequency is equivalent to about −0.06e (from inset of Figure 4b), which is much smaller than the charge

dx.doi.org/10.1021/nl501805e | Nano Lett. XXXX, XXX, XXX−XXX

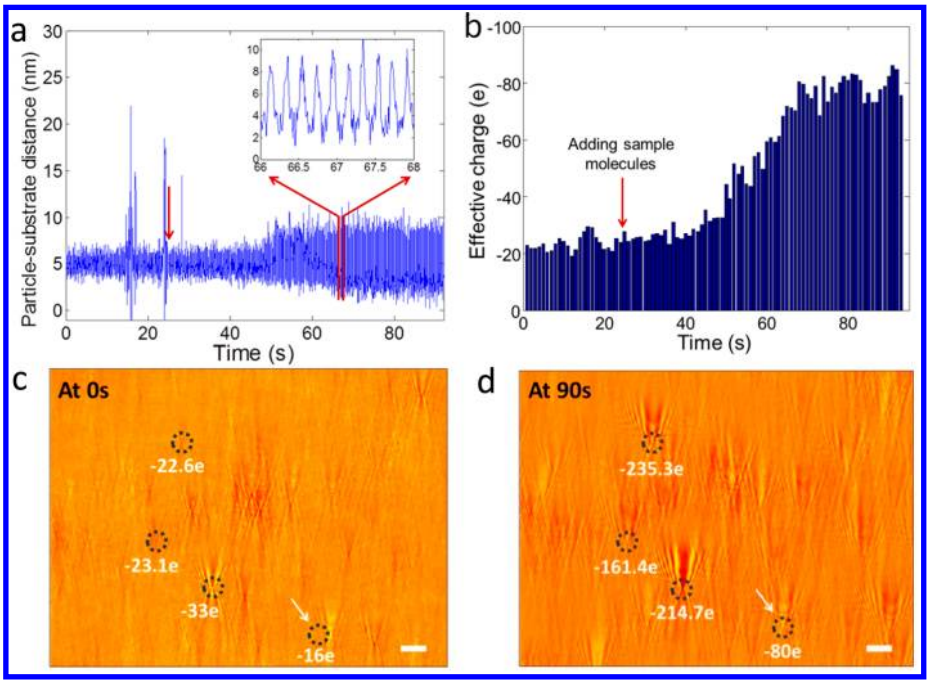

Figure 5. (a) Response of a nano-oscillator to the binding of biotin-PEG-COOH, where the arrow points the introduction of the sample molecule. The nano-oscillator is marked by a white arrow in (c,d). Inset: Zooming-in of the oscillation. (b) Effective charge of the nano-oscillator during the molecular binding process. Note that the spikes at 16 and 24 s in (a) were caused by mechanical perturbation associated with sample introduction. (c,d) Effective charges of different nano-oscillators before and 90 s after the introduction of the molecules. The images were obtained by taking the imaginary part of the Fourier transform for each pixel at t = 0 and 90 s, respectively. Applied electric field: amplitude = 5 V/m and frequency = 5 Hz. Buffer: 10 mM PBS solution. Molecular tether: PEG with molecular mass of 3400 g/mol. Sample introduction: 1 μL of 1 mM biotin-PEG-COOH added to 300 μL of 10 mM PBS buffer solution. Scale bars: 5 μm.

fluctuations of nano-oscillators #1 and #2. This indicates that the fluctuations of nano-oscillators #1 and #2 in Figure 4b were due to charge fluctuations rather than Brownian motion. The inset of Figure 4d compares the effective charge of a nano-oscillator and the equivalent charge noise due to Brownian motion, which shows that the current detection limit is sufficient to detect a single electron charge. In fact, if taking the detection limit as 3 times of the Brownian motion noise, then the present method can detect 0.18e charge.

Each of the nano-oscillators can serve as a sensor to detect molecular binding events. When a charged molecule binds onto the AuNP of a nano-oscillator, the total charge of the AuNP changes, which can be readily detected. Even in the case of uncharged molecules, the binding may affect the surface charge distribution of the AuNP, which may also be detected. To demonstrate the ability of the nano-oscillators for molecular detections, we studied the binding of biotin-PEG-COOH molecules to the nano-oscillators. To evaluate the nano-oscillator's potential biosensor applications, we used 10 mM PBS as buffer solution. Although ionic screening due to the buffer lowers the oscillation amplitude, we are still able to detect the charge of nano-oscillators at relative high ionic strengths (e.g., 20 mM; see Supporting Information). Figure 5a shows the oscillation of a 30 nm diameter nano-oscillator (marked by an arrow in Figure 5c,d) during the binding process, where the spikes pointed by the arrow are due to the introduction and mixing of the sample solution in 10 mM PBS. Despite the mechanical perturbation, the oscillation signal is not affected by the introduction of the sample solution. As the binding takes place, the oscillation amplitude increases, corresponding to the increase in the negative charges of the AuNP. This is expected because biotin-PEG-COOH molecules are negatively charged. Figure 5b shows the change of the AuNP during the binding process. Before the binding, the nano-oscillator has about −16.5 charges. After the binding process, the charge of the nano-oscillator changes to −80e. From the change of the charge, we estimate that the number of biotin-PEG-COOH molecules is about 166 after considering ionic screening.

The oscillation of other nano-oscillators has also been followed over time. Figure 5c shows the effective charges of 4 nano-oscillators before exposure to biotin-PEG-COOH. The binding of biotin-PEG-COOH causes effective charge changes for all the nano-oscillators, but the amount of the changes and detailed kinetics are different for different nano-oscillators. The surface density of the nano-oscillators was controlled to be ~1500/mm^2 in the present work by introducing spacers between the nano-oscillators. The limit is determined by the spatial resolution of the imaging technique, which is about 300 nm. So in principle, much higher density arrays of nano-oscillators can be prepared and detected simultaneously with the plasmonic imaging technique. The high-density array and parallel plasmonic detection, together with single charge detection limit, promise high throughput and sensitive detection and study of molecular interactions.

In conclusion, nano-oscillators have been fabricated by attaching nanoparticles to a surface with molecular tethers. By applying an electric field applied perpendicular to the surface, the individual nano-oscillators are driven into oscillations, which can be measured individually with ~0.1 nm accuracy with a plasmonic imaging technique. From the oscillation amplitude and phase, the charge of each nano-oscillator has been determined with an accuracy of ~0.18 electron charges along with the charge polarity. In aqueous buffer solutions,

dx.doi.org/10.1021/nl501805e | Nano Lett. XXXX, XXX, XXX−XXX

ionic screening of the charge affects the oscillation amplitude, but sensitive detection of charges at relative high ionic strength buffers (e.g., 20 mM) is still possible, which is useful for potential biological applications. To demonstrate applications, the self-assembled nano-oscillators have been used to detect molecular binding onto the nanoparticles. These capabilities will open the door to the detection of molecules, including small molecule binding and post-translational modification of proteins without labels. The work demonstrates a bottom-up approach to fabricate high-density NEMS, and a sensitive method to detect the individual NEMS in parallel.

■ ASSOCIATED CONTENT

Supporting Information

Fabrication of nano-oscillators, driving the nano-oscillators, optical setup, signal processing, nanoparticle−substrate distance calibration and detection limit, Brownian motion, overdamped oscillator model, zeta-potential and solution conductivity measurement, charge screen effect, and Movies S1−3. This material is available free of charge via the Internet at http://pubs.acs.org.

■ AUTHOR INFORMATION

Corresponding Author

*E-mail: njtao@asu.edu.

Author Contributions

X.N.S. carried out the experiments and analyzed the data, Y.M.F. and S.W. helped sample preparation and some experiments, S.W. helped with instrumentation, Y.G. helps theoretical modeling, H.Y.C. helped to supervise the project, N.J.T. conceived and supervised the project, and X.N.S. and N.J.T. wrote the paper.

Notes

The authors declare no competing financial interest.

■ ACKNOWLEDGMENTS

We thank Keck Foundation and Gordon and Betty Moore.

■ REFERENCES

(1) Levene, M. J.; Korlach, J.; Turner, S. W.; Foquet, M.; Craighead, H. G.; Webb, W. W. *Science* **2003**, *299*, 682−686.
(2) Schedin, F.; Geim, A. K.; Morozov, S. V.; Hill, E. W.; Blake, P.; Katsnelson, M. I.; Novoselov, K. S. *Nat. Mater.* **2007**, *6*, 652−655.
(3) Punj, D.; Mivelle, M.; Moparthi, S. B.; van Zanten, T. S.; Rigneault, H.; van Hulst, N. F.; Garcia-Parajo, M. F.; Wenger, J. *Nat. Nanotechnol.* **2013**, *8* (7), 512−516.
(4) Armani, A. M.; Kulkarni, R. P.; Fraser, S. E.; Flagan, R. C.; Vahala, K. J. *Science* **2007**, *317*, 783−787.
(5) Bonifas, A. P.; McCreery, R. L. *Nat. Nanotechnol.* **2010**, *5*, 612−617.
(6) Favier, F.; Walter, E. C.; Zach, M. P.; Benter, T.; Penner, R. M. *Science* **2001**, *293*, 2227−2231.
(7) Turner, A. P. F. *Science* **2000**, *290*, 1315−1317.
(8) Wu, G. H.; Datar, R. H.; Hansen, K. M.; Thundat, T.; Cote, R. J.; Majumdar, A. *Nat. Biotechnol.* **2001**, *19*, 856−860.
(9) Burg, T. P.; Godin, M.; Knudsen, S. M.; Shen, W.; Carlson, G.; Foster, J. S.; Babcock, K.; Manalis, S. R. *Nature* **2007**, *446*, 1066−1069.
(10) Anker, J. N.; Hall, W. P.; Lyandres, O.; Shah, N. C.; Zhao, J.; Van Duyne, R. P. *Nat. Mater.* **2008**, *7*, 442−453.
(11) Ament, I.; Prasad, J.; Henkel, A.; Schmachtel, S.; Sonnichsen, C. *Nano Lett.* **2012**, *12*, 1092−1095.
(12) Zijlstra, P.; Paulo, P. M. R.; Orrit, M. *Nat. Nanotechnol.* **2012**, *7*, 379−382.
(13) Murray, B. J.; Walter, E. C.; Penner, R. M. *Nano Lett.* **2004**, *4*, 665−670.
(14) Millikan, R. A. *Science* **1910**, *32*, 436−448.
(15) Cleland, A. N.; Roukes, M. L. *Nature* **1998**, *392*, 160−162.
(16) Yang, Y. T.; Callegari, C.; Feng, X. L.; Ekinci, K. L.; Roukes, M. L. *Nano Lett.* **2006**, *6*, 583−586.
(17) Morarad, N.; Krishnan, M. *Nat. Nanotechnol.* **2012**, *7*, 448−452.
(18) Krishnan, M.; Mojarad, N.; Kukura, P.; Sandoghdar, V. *Nature* **2010**, *467*, 692−696.
(19) Shan, X. N.; Patel, U.; Wang, S. P.; Iglesias, R.; Tao, N. J. *Science* **2010**, *327*, 1363−1366.
(20) MacGriff, C.; Wang, S. P.; Wiktor, P.; Wang, W.; Shan, X. N.; Tao, N. J. *Anal. Chem.* **2013**, *85*, 6682−6687.
(21) Shan, X. N.; Huang, X. P.; Foley, K. J.; Zhang, P. M.; Chen, K. P.; Wang, S. P.; Tao, N. J. *Anal. Chem.* **2010**, *82*, 234−240.
(22) Mock, J. J.; Hill, R. T.; Tsai, Y. J.; Chilkoti, A.; Smith, D. R. *Nano Lett.* **2012**, *12*, 1757−1764.
(23) Wang, Y.; Zocchi, G. *Phys. Rev. Lett.* **2010**, 105.
(24) Rothenhausler, B.; Knoll, W. *Nature* **1988**, *332*, 615−617.
(25) Huang, B.; Yu, F.; Zare, R. N. *Anal. Chem.* **2007**, *79*, 2979−2983.
(26) Wang, S. P.; Shan, X. N.; Patel, U.; Huang, X.; Lu, J.; Li, J.; Nongjian, T. *Proc. Natl. Acad. Sci. U.S.A.* **2010**, *107*, 16028−16032.
(27) Shan, X.; Diez-Perez, I.; Wang, L.; Wiktor, P.; Gu, Y.; Zhang, L.; Wang, W.; Lu, J.; Wang, S.; Gong, Q.; Li, J.; Tao, N. *Nat. Nanotechnol.* **2012**, *7*, 668−672.
(28) Yu, H.; Shan, X. N.; Wang, S. P.; Chen, H. Y.; Tao, N. J. *ACS Nano* **2014**, *8*, 3427−3433.
(29) Jain, P. K.; Huang, W. Y.; El-Sayed, M. A. *Nano Lett.* **2007**, *7*, 2080−2088.
(30) Jain, P. K.; El-Sayed, M. A. *Nano Lett.* **2007**, *7*, 2854−2858.
(31) Wei, Q. H.; Su, K. H.; Durant, S.; Zhang, X. *Nano Lett.* **2004**, *4*, 1067−1071.
(32) Wang, K.; Schonbrun, E.; Crozier, K. B. *Nano Lett.* **2009**, *9*, 2623−2629.
(33) Ma, C.; Contento, N. M.; Gibson, L. R.; Bohn, P. W. *Anal. Chem.* **2013**, *85*, 9882−9888.
(34) Feng, J.; Siu, V. S.; Roelke, A.; Mehta, V.; Rhieu, S. Y.; Palmore, G. T. R.; Pacifici, D. *Nano Lett.* **2012**, *12*, 602−609.
(35) Yeh, W. H.; Hillier, A. C. *Anal. Chem.* **2013**, *85*, 4080−4086.
(36) Wang, W.; Foley, K.; Shan, X.; Wang, S. P.; Eaton, S.; Nagaraj, V. J.; Wiktor, P.; Patel, U.; Tao, N. J. *Nat. Chem.* **2011**, *3*, 249−255.
(37) Lu, J.; Wang, W.; Wang, S. P.; Shan, X. N.; Li, J. H.; Tao, N. J. *Anal. Chem.* **2012**, *84*, 327−333.
(38) Shan, X.; Wang, S.; Tao, N. *Appl. Phys. Lett.* **2010**, *97*, 223703.
(39) Ly, N.; Foley, K.; Tao, N. J. *Anal. Chem.* **2007**, *79*, 2546−2551.
(40) Ciraci, C.; Hill, R. T.; Mock, J. J.; Urzhumov, Y.; Fernandez-Dominguez, A. I.; Maier, S. A.; Pendry, J. B.; Chilkoti, A.; Smith, D. R. *Science* **2012**, *337*, 1072−1074.
(41) Hill, R. T.; Mock, J. J.; Hucknall, A.; Wolter, S. D.; Jokerst, N. M.; Smith, D. R.; Chilkoti, A. *ACS Nano* **2012**, *6*, 9237−9246.
(42) Foley, K. J.; Shan, X.; Tao, N. J. *Anal. Chem.* **2008**, *80*, 5146−5151.
(43) Shan, X. N.; Wang, S. P.; Wang, W.; Tao, N. J. *Anal. Chem.* **2011**, *83*, 7394−7399.
(44) Oesterhelt, F.; Rief, M.; Gaub, H. E. *New J. Phys.* **1999**, *1*, 11.
(45) Diamandis, E. P.; Christopoulos, T. K. *Clin. Chem.* **1991**, *37*, 625−636.
(46) Morrison, I. D.; Ross, S. *Colloidal Dispersions: Suspensions, Emulsions, and Foams*; John Wiley and Sons: New York, 2002.
(47) O'Brien, R. W. *J. Colloid Interface Sci.* **1983**, *92*, 204−216.